Revealing the effect of conductive mechanism on the voltage endurance of ferroelectric thin films *via* controlling deposition temperature for reaching high energy storage capability

Hongmei Jing[a], Shibo Zhao[a] Ting Wang[b], Wanbiao Hu[c*], Liming Diwu[d], Jingru Xu[d]*

Miao Liu[e], Zhuo Wang[f], Zixiong Sun[df*]*

a School of Physics and Information Technology, Shaanxi Normal University, Xi'an, 710119, PR China

b Guangdong Provincial Key Laboratory of Electronic Functional Materials and Devices, Huizhou University, Huizhou 516001, Guangdong, China.

c Yunnan Key Laboratory of Electromagnetic Materials and Devices

d School of Electronic Information and Artificial Intelligence, Shaanxi University of Science and Technology, Xi'an 710021, PR China

e Institute of Industrial Hygiene of Ordance Industry, Xi'an Shaanxi 710065, China

f School of Materials Science and Engineering, Shaanxi University of Science and Technology, Xi'an 710021, PR China

---

**Corresponding author: Hongmei Jing, Zhuo Wang, Zixiong Sun*

E-mail address: jhmei.dengdai@snnu.edu.cn, SunZX@sust.edu.cn, wangzhuo@sust.edu.cn.

Supplementary Information

1. *Experimental Section*

1.1 Deposition conditions:

The stoichiometric target of $0.75Ba_{0.15}Ca_{0.85}Zr_{0.1}Ti_{0.9}O_3$-$0.15Bi(Zn_{2/3}Ta_{1/3})O_3$(BCZT-BZT) was fabricated by the authors using conventional solid-state technology. this composition was chosen because our previous study indicated that ceramic bulk of the same composition exhibited outstanding energy storage performance, which motivated us to further investigate the structure-function relationship[1][2]. The $SrRuO_3$(SRO) target was purchased from the *SurfaceNet*, and $SrTiO_3$ (001) substrates were purchased from *CrystTec*. The target surface was manually polished with sandpaper. The grinding residue was blown off with a nitrogen gun. The SRO layer was grown by pulsed laser deposition (PLD) at 650 ^oC under the oxygen pressure of 0.13 mbar using a *KrF* excimer laser (*LPX 205, Coherent*) with a laser frequency of 5 Hz, resulting in the thickness of about 100 nm. The BCZT-BZT thin film was subsequently deposited in the same chamber with different deposition temperatures of 600 ^oC, 650 ^oC, 700 ^oC, and 750 ^oC, respectively, under the oxygen pressure of 0.1 mbar, and the frequency remained at 5 Hz. In general, comparing the energy storage performance of dielectric films requires all the samples having the same thickness, and the films' growth is sensitive to the temperature. In this case, the thickness of all the films were controlled to be equal by adjusting the deposition time, and the thickness was around 700 nm. The annealing process was performed *in situ* at

650 ^{o}C under 10 mbar oxygen pressure directly after the deposition in the same chamber for 20 min.

1.2 Characterizations and measurements:

X-ray diffraction analysis was performed using a *PANalytical X'Pert³ MRD* diffractometer, using 2*θ*-*ω* scans, *phi*-scans, *X*-ray reflectivity, and reciprocal space mapping (RSM). For 2*θ*-*ω* scans, the *Step size* and *Time per step* are 0.0005^{o} and 0.5 s, respectively. For RSM mappings, the *Step size* of *2θ* axis and *ω* axis are all 0.02^{o,} and the *Time per step* of *2θ* axis is 20 s. The high-angle transmission electron microscope annular dark field (HR-TEM HAADF) measurements were performed by transmission electron microscopy (*FEI Titan Cubed Themis G2 300*), and the electrons source is field-emission source. The *ε*-*f* with *tanδ*-*f* curves and *I*-*V* results were collected with a Keithley 4200 LCR meter. Dielectric constants were calculated using the formula of $C = \frac{\varepsilon S}{4k\pi d}$. The *I*-*V* measurements were carried out using a top-to-bottom mode, as sketched in Fig. S2. The ferroelectric hysteresis (*P*-*E*) loops were measured by the ferroelectric tester with the mode of *aixACCT TF2000E*. The regular *P*-*E* loops were measured at 1000 Hz with unipolar mode.

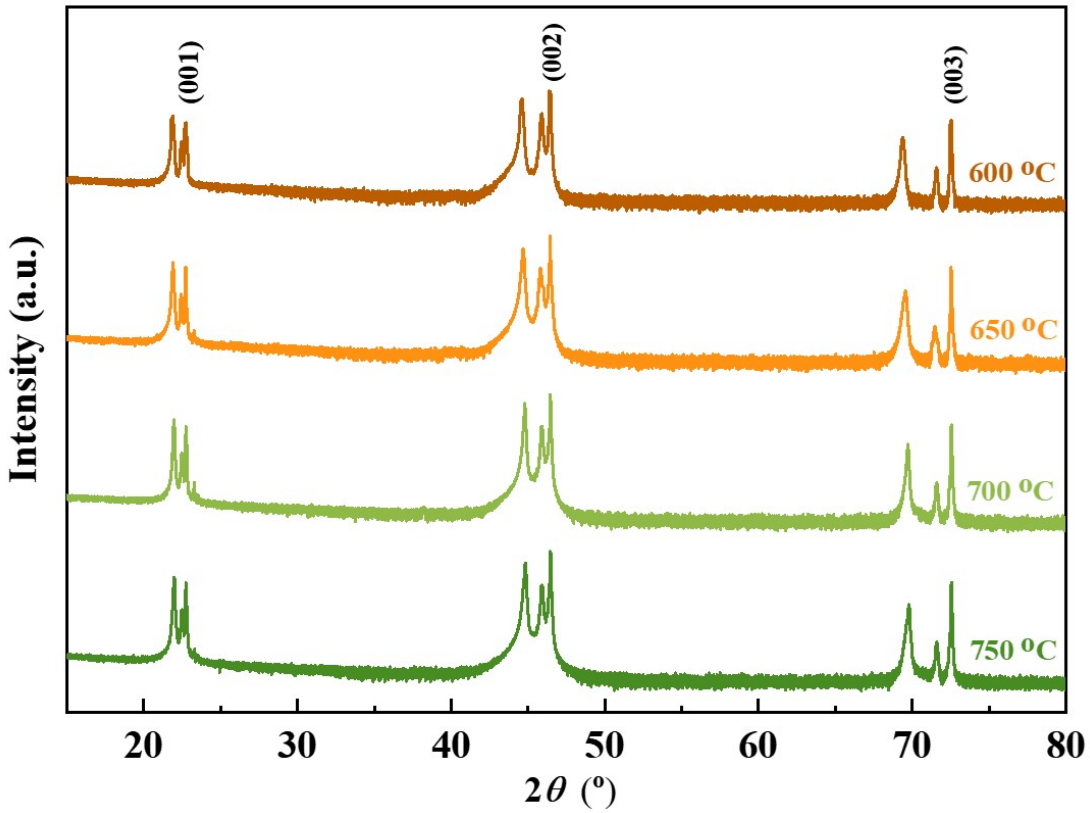

Figure S1 the 2θ-ω scans of all the BCZT-BZT thin films from 15° to 80°.

2. *Gaussian-LorenCross Function*

$$y = y_0 + \frac{A}{1 + \frac{e^{\frac{0.5(1-s)(x-x_c)^2}{w^2}}}{\frac{s(x-x_c)^2}{w^2}}} \qquad \text{Eq. S1}$$

The y_0, x_c, A, w, and s are the base, center, amplitude, width, and shape of each peak, respectively. The maximum number of iterations and the tolerance of the fitting process are 200 and $1e^{-6}$, respectively, which indicate very high reliability[3].

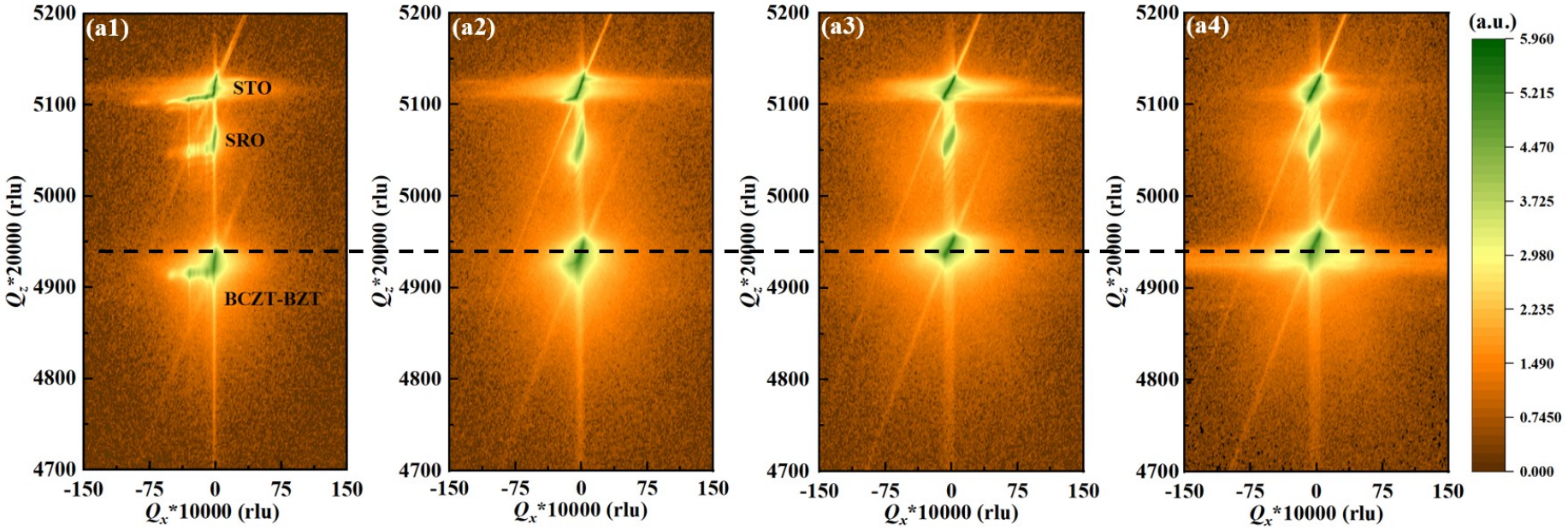

Figure S2 the RSMs around the (001) plane of all the BCZT-BZT films

3. *Weibull* distribution method

Before calculating the energy storage density(W_{rec}), the electric breakdown strength(E_b) of each film should be confirmed by employing the *Weibull* distribution, which can be expressed as follows:

$$X_i = \ln E_i \quad \text{Eq. S2}$$

$$Y_i = \ln(- \ln (1 - P_i)) \quad \text{Eq. S3}$$

$$P_i = \frac{i}{1 + n} \quad \text{Eq. S4}$$

Where X_i and Y_i are the two parameters of the Weibull distribution, Y_i varies linearly with X_i with a slope of β, $E_{i,}$ and P_i are the sample's breakdown field and the electric field's failure probability distribution, respectively. While n, i, and β are the total number of specimens, the serial number of dielectric strength, and the slope of the linear relationship between $\ln(E_i)$ and $\ln(-\ln(1-P_i))$, respectively.

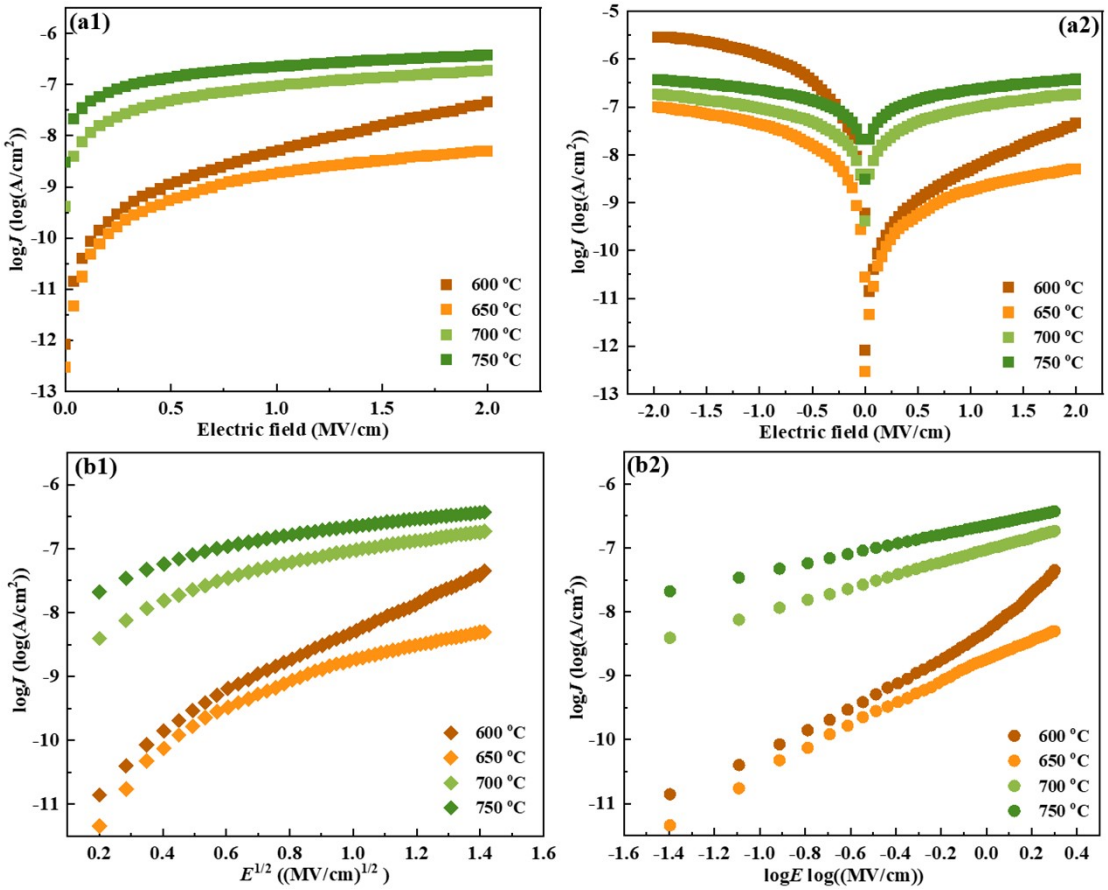

Fig. S3 (a1) the one-side *J-E* curves (a2) the two-side *J-E* curves of all the BCZT-BZT thin films; the fitting curve of Fig. S3(a) according to the (b1) Schottky emission; (b2) Ohmic contact.

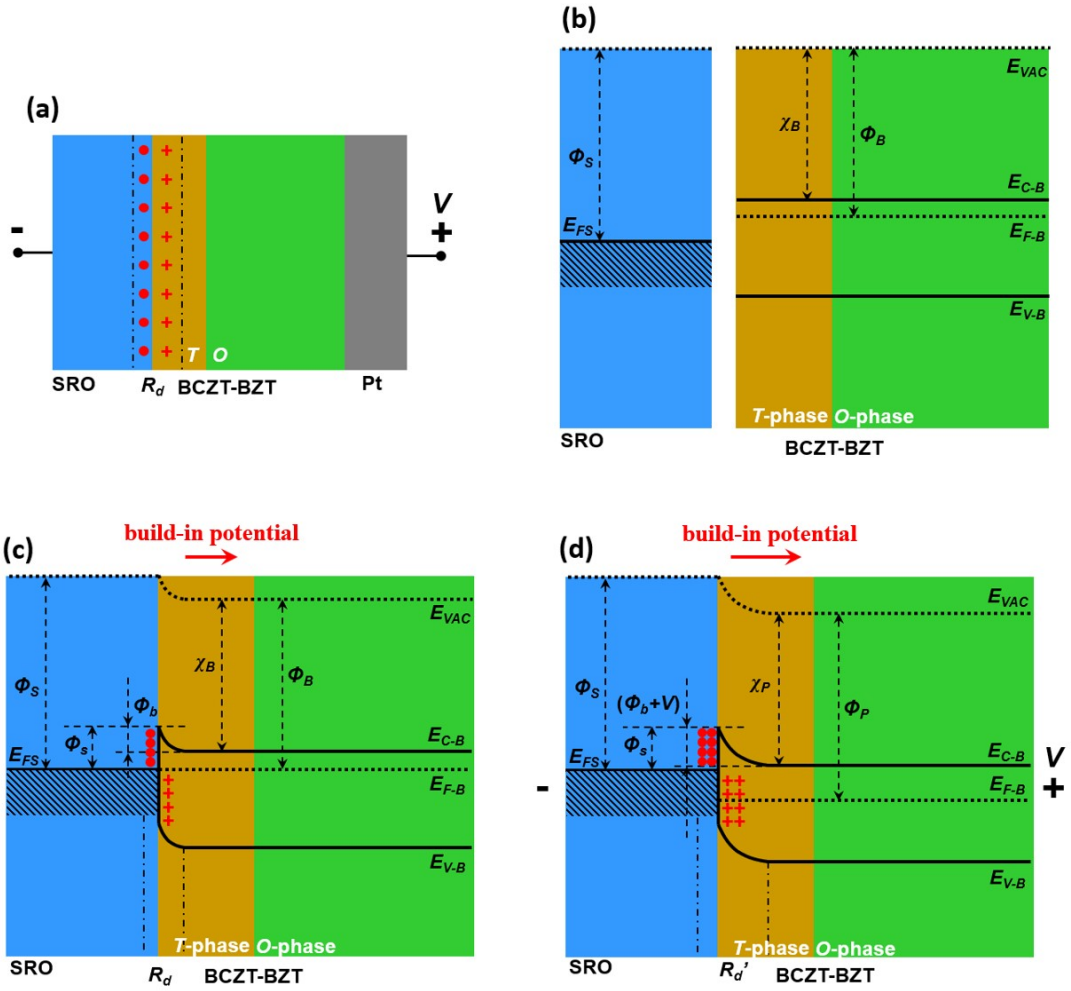

Figure S4 (a) equivalent circuit of the Pt/BCZT-BZT65/SRO heterostructure; (b) the band diagram of the SRO/BCZT-BZT65 interface before contact; (c) the band diagram of the SRO/BCZT-BZT65 interface after contact; the band diagram of the SRO/BCZT-BZT65 interface under forward bias.

4. Explanation of the *Schottky* barrier formation

Figure S4(a) illustrates the equivalent circuit of the Pt/BCZT-BZT65/SRO heterostructure, where the Pt, BCZT-BZT, and SRO are considered as three components connected in series. Since the depletion layer forms only at the interface between the SRO and the film, our discussion will focus on this side. Additionally, Schottky emission was observed only in BCZT-BZT60 and BCZT-BZT65, thus the discussion in this section is limited to these two thin films. Figure S4(b) presents the band diagram of the SRO/BCZT-BZT65 interface before contact. Given that the work function of SRO (over 5.0 eV) is consistently higher than the electron affinity of $BaTiO_3$-based systems, the Fermi levels of both SRO and BCZT-BZT65 align when connected[4][5], which leads to band bending in the interface, as shown in Fig. S4(c). Since the majority carriers in such systems are electrons, the film can be regarded as an *n*-type semiconductor. In this scenario, electrons drift from the film to the SRO and become trapped there, forming a depletion layer (Φ_b) at the interface and inducing a built-in potential (Φ_b) directed from the SRO to the film. When a forward external voltage (V) is applied, pointing from the film to the SRO, as depicted in Figure S4(d), the Fermi level of BCZT-BZT65 shifts downwards, increasing Φ_b to Φ_b+V and R_d to R_d'. Consequently, more electrons become trapped at the interface, increasing the forward resistivity of the BCZT-BZT65 film.

5. Electric field redistribution

Assume that the voltage applied on the BCZT-BZT thin film is U. Because the films is composed of T-phase, C-phase, and O-phase, and due to the thickness of the C-phase is too thin(only several unit cell), which can be ignored, the electric field redistribution can be simplified as only happens on the T-phase and O-phase, and the film can be considered as two capacitors connected in series. So first we can have

$$U = U_T + U_O \qquad \text{Eq. S5}$$

where the U_T and U_O are the partial voltage applied on the T-phase and O-phase, respectively. Then we can have

$$U_T = E_T d_T \quad U_0 = E_O d_O \qquad \text{Eq. S6}$$

where the E_T, E_O and d_T, d_O are the electrical fields of and the equivalent thickness of each phase, respectively. According to the law of conservation of charge, the surface charge(Q) of each capacitor should be equal. Considering the relationship between Q, U, and C, and the definition of capacitance, the inversely proportional relationship between dielectric constant and applied partial voltage can be deduced as follows:[6]

$$Q_T = Q_O \qquad \text{Eq. S7}$$

$$Q = CU \qquad \text{Eq. S8}$$

$$C_T U_T = C_O U_O \qquad \text{Eq. S9}$$

$$C = \frac{\varepsilon_r S}{4k\pi d} \qquad \text{Eq. S10}$$

$$\frac{C_T}{C_O} = \frac{U_O}{U_T} = \frac{\varepsilon_{rT}}{\varepsilon_{rO}} \cdot \frac{d_0}{d_T} \qquad \text{Eq. S11}$$

According to the definition, the ε_r consists of a real part (ε_r') and an imaginary part (ε_r''), which be written as:

$$\varepsilon_r = \varepsilon_r' + j\varepsilon_r'' \quad \text{Eq. S12}$$

and the ratio between them is defined as the loss tangent value ($tan\delta$), which also means the dielectric loss factors in a dielectric relaxation process.

$$tan\,\delta = \frac{\varepsilon_r''}{\varepsilon_r'} \quad \text{Eq. S13}$$

Thus the Eq. S12 can be written as:

$$\varepsilon_r = \varepsilon_r' + j\varepsilon_r'' = \varepsilon_r'(1 + jtan\,\delta) \quad \text{Eq. S14}$$

Based on some previous literature, the relationship between the ε_r' and the AC conductivity (σ) is derived in terms of the following formulas[7]:

$$\sigma = \omega\varepsilon_0\varepsilon_r' tan\,\delta = \omega\varepsilon_0\varepsilon_r'' \quad \text{Eq. S15}$$

in which the ε_0 is the vacuum permittivity with the value of ε_0=8.85×10^{-14} F/cm. Considering the ω and σ are expressed as:

$$\omega = 2\pi f, \rho = 1/\sigma \quad \text{Eq. S16}$$

where ρ and f are the resistivity of the dielectric and frequency of the applied electrical field. Combine Eq. S14-16 and finally, we can have the inversely proportional relationship between resistivity and dielectric constant.

$$\frac{1}{\rho} = \frac{2\pi f\varepsilon_0\varepsilon_r tan\,\delta}{(1 + jtan\,\delta)} \quad \text{Eq. S17}$$

In this work, the BCZT-BZT60 and BCZT-BZT65 obey the Schottky emission, which means that there should have depletion layer at the bottom of the film. And because the depletion layer is too thin that only exists in the *T*-phase. Thus, the

resistivity increment of BCZT-BZT60 and BCZT-BZT65 thin films actually happens in the *T*-phase. As expressed in Eq. S17, increasing the resistivity of the *T*-phase decreases its ε_r, and because the thickness of *T*-phase and *O*-phase is fixed, the voltage applied in the *T*-phase increases. Such a phenomenon can be seen as the electric field redistribution. Based on the RSMs around the (103) plane of the BCZT-BZT films, the thickness of the *T*-phase in BCZT-BZT60 and BCZT-BZT65 is much thicker than that of BCZT-BZT70 and BCZT-BZT75, thus such a field redistribution increases the voltage endurance of BCZT-BZT60 and BCZT-BZT65, which own higher E_b than BCZT-BZT70 and BCZT-BZT75.

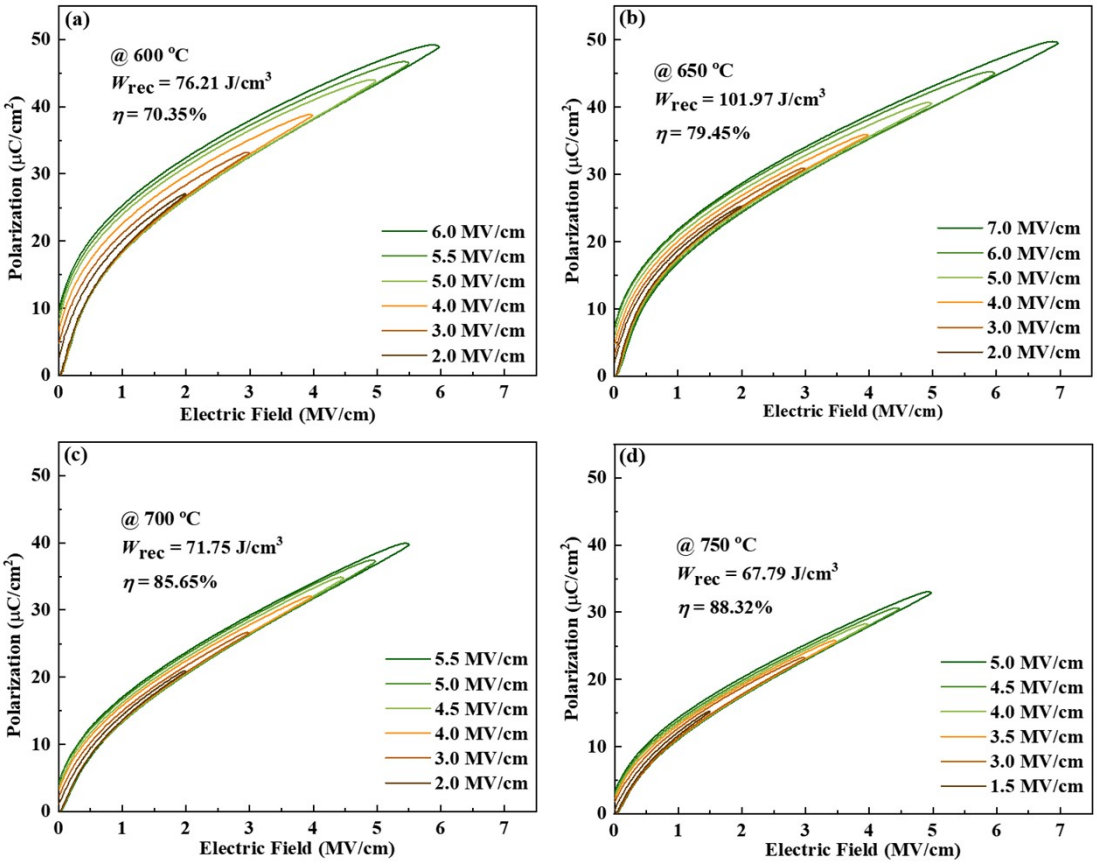

Figure S5 the *P-E* loops of BCZT-BZT thin films under different applied fields with different deposition temperatures

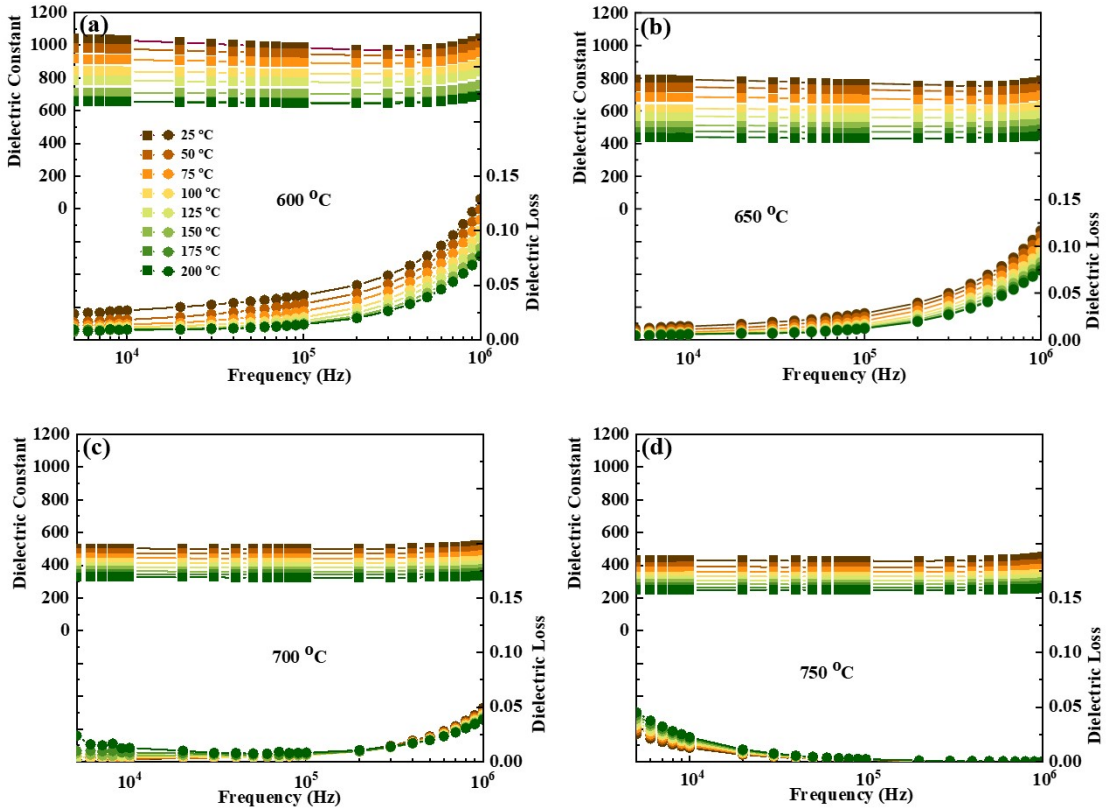

Figure S6 the *ε-f* and *tanδ-f* curves from 25 °C to 200 °C for all the BCZT-BZT thin films

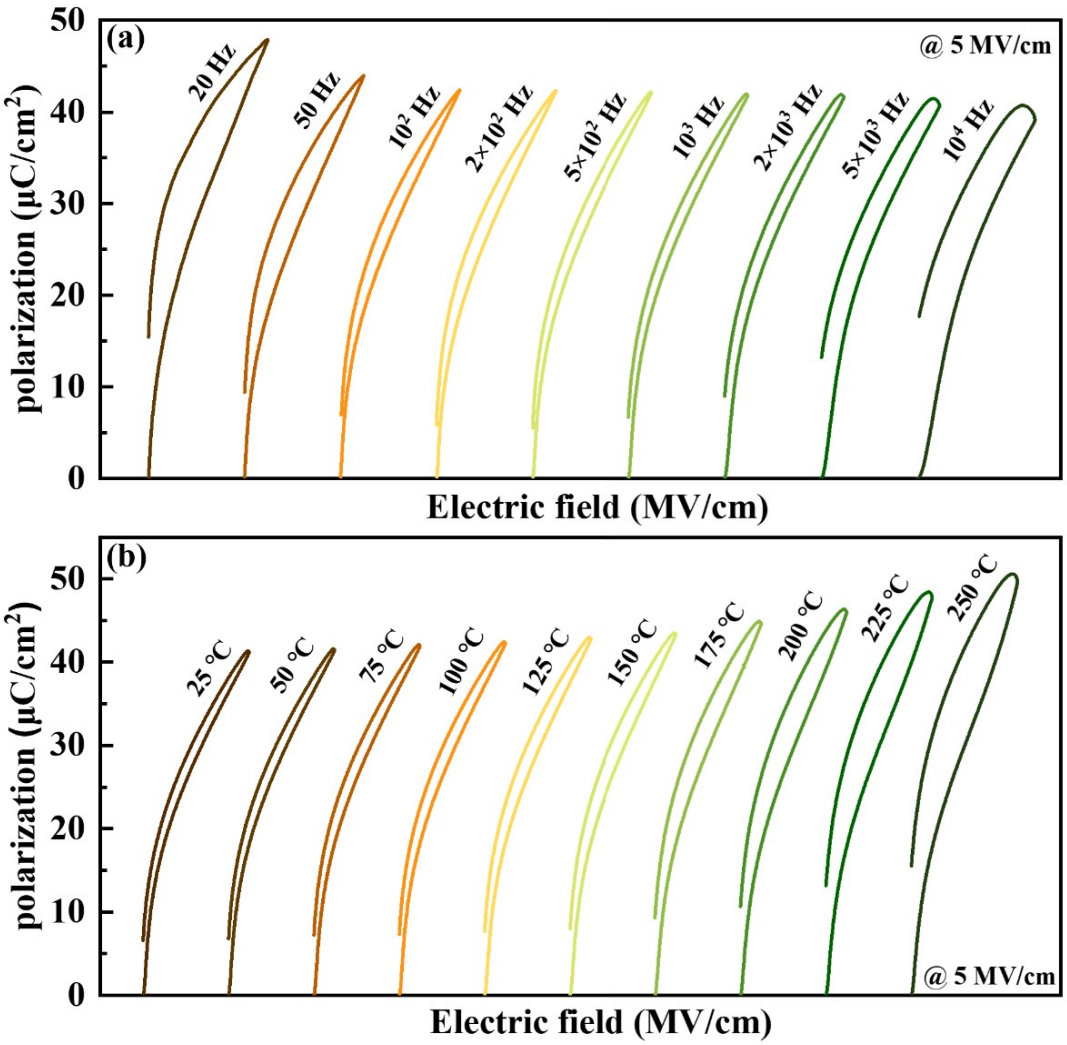

Figure S7 (a) the *P*-*E* loops of the BCZT-BZT65 measured at 5.0 MV/cm (a) from 20 Hz to 10^4 Hz at room temperature; (b) from 25 °C to 250 °C at 1 kHz.

References

[1] Sun, Z.; Bai, Y.; Jing, H.; Hu, T.; Du, K.; Guo, Q.; Gao, P.; Tian, Y.; Ma, C.; Liu, M.; Pu, Y. A Polarization Double-Enhancement Strategy to Achieve Super Low Energy Consumption with Ultra-High Energy Storage Capacity in BCZT-Based Relaxor Ferroelectrics. *Mater. Horiz.* **2024**. *11* (14), 3330-3344.

[2] Sun, Z.; Zhao, S.; Wang, T.; Jing, H.; Guo, Q.; Gao, R.; Diwu, L.; Du, K.; Hu, Y.; Pu, Y. Achieving High Overall Energy Storage Performance of KNN-Based Transparent Ceramics by Ingenious Multiscale Designing. *J. Mater. Chem. A.* **2024**. *12* (27), 16735-16747.

[3] Sun, Z.; Huang, S.; Zhu, W.; Birkhölzer, Y. A.; Gao, X.; Avila, R. A.; Huang, H.; Lou, X.; Houwman, E. P.; Nguyen, M. D.; Koster, G.; Rijnders, G. Structure Evolution of the Interfacial Layer of $BaTiO_3$ Thin Films during Annealing Process and Related Good Resistive Switching Behaviors. *Appl. Phys. Lett. Mater.* **2023**, *11* (10), 101129.

[4] Grebinskij, S.; Masys, Š.; Mickevičius, S.; Lisauskas, V.; Jonauskas, V. Ab Initio and Photoemission Study of Correlation Effects in $SrRuO_3$ Thin Films. *Phys. Rev. B.* **2013**, *87* (3), 035106.

[5] Fang, X.; Kobayashi, T. Study of Pulsed Laser Deposition of RuO_2 and $SrRuO_3$ Thin Films. *Appl Phys A.* **1999**, *69* (1), S587–S590.

[6] Moon, H.; Cho.; S. K.; Garrell,; R. L.; Kim.; C. J. Low Voltage Electrowetting-on-Dielectric. *J. Appl. Phys*. **2002**, *92* (7), 4080-4087.

[7] Shaikh, P. A.; Shi, D.; Retamal, J. R. D.; Sheikh, A. D.; Haque, M. A.; Kang, C.-F.; He, J.-H.; Bakr, O. M.; Wu, T. Schottky Junctions on Perovskite Single Crystals: Light-Modulated Dielectric Constant and Self-Biased Photodetection. *J. Mater. Chem. C.* **2016**, *4* (35), 8304–8312.